ARTICLE

Energy Transfer and Electron Transfer in Composite System of Carbon Quantum Dots/Rhodamine B Molecules

Kang Wei, Lei Zhang, Shen-long Jiang, Qun Zhang*

Hefei National Laboratory for Physical Sciences at the Microscale, Department of Chemical Physics, and Synergetic Innovation Center of Quantum Information & Quantum Physics, University of Science and Technology of China, Hefei 230026, China

(Dated: Received on May 27, 2019; Accepted on June 4, 2019)

In this work, we investigated the energy transfer (EnT) and electron transfer (ET) processes as well as their relationship in the carbon quantum dots/rhodamine B (CQDs/RhB) including *o*-CQDs/RhB and *m*-CQDs/RhB systems by using photoluminescence spectroscopy in combination with steady-state and transient absorption spectroscopy. We found that the ET process is negligible in the *o*-CQDs/RhB system with an EnT efficiency as high as 73.2%, while it becomes pronounced in the *m*-CQDs/RhB system whose EnT efficiency is lower than 33.5%. Such an interplay of EnT and ET processes revealed in the prototypical composite system consisting of carbon quantum dots and dye molecules would provide helpful insights for applications of relevance to exciton quenching.

Key words: Carbon quantum dots, Rhodamine B molecules, Energy transfer, Electron transfer, Photoluminescence spectroscopy, Ultrafast transient absorption spectroscopy

I. INTRODUCTION

In the field of photophysics and photochemistry of relevance to quantum dots (QDs), it is highly desirable to look into the photoexcited exciton dynamics involved in the system, as this examination can provide mechanistic insights into the QDs-based materials including (but not limited to) solar cells, light-emitting diodes, and photocatalysts [1−3]. Specifically, in terms of the QDs-based photocatalysis, the understanding of exciton quenching kinetics is rather instructive for achieving performance improvement of the photocatalytic system. The present investigations of exciton quenching kinetics are mainly focused on either energy transfer (EnT) [4, 5] or electron transfer (ET) [6, 7] processes. As is well known, the organic dye molecules in the excited state are commonly used as the energy acceptor in an EnT system, due to their inherent advantages such as good solubility, excellent photostability, high extinction coefficient, and high photoluminescence (PL) quantum yield [8]. In terms of the composite systems consisting of QDs and dye molecules, one can readily find numerous reports on the behavior of exciton quenching of QDs through either EnT [9−11] or ET [12−14] processes. For instance, Sadhu and coworkers studied the EnT process in the composite system consisting of CdSe QDs and Nile red dye molecules [10], Jagadeeswari and coworkers studied the ET process in the composite system consisting of CdTe QDs and anthraquinone dye molecules [13]. Notably, however, the investigations of the relationship between the EnT and ET processes in the alike composite systems consisting of QDs and dye molecules remain rather limited.

In this work, we employed steady-state absorption and photoluminescence (PL) spectroscopy as well as ultrafast transient absorption (TA) spectroscopy to examine the EnT and ET processes as well as their relationship in a prototypical composite system consisting of carbon quantum dots and rhodamine B molecules (denoted CQDs/RhB hereafter). The two different CQDs, *i.e.*, *o*-CQDs and *m*-CQDs, were deliberately synthesized from the two precursors, *i.e.*, *o*-phenylenediamine and *m*-phenylenediamine, respectively. By virtue of the different spectral overlaps between the PL emission profiles of the two CQDs and the absorption profile of RhB, the efficiencies of EnT from the donor CQDs to the acceptor RhB should be different for the two composite systems. On the basis of analyses using Förster model, we found that the EnT efficiency in *o*-CQDs/RhB (∼73.2%) is more than twice that in *m*-CQDs/RhB (∼33.5%). On the other hand, given the relative energetics among *o*-CQDs, *m*-CQDs, and RhB, the ET process can also take place from each CQDs to RhB. On the basis of analyses of the ultrafast TA results, we revealed that the ET behavior is negligible in the *o*-CQDs/RhB system while it becomes pronounced in the *m*-CQDs/RhB system. Such an observed interplay of "one wanes and the other waxes" would be a general case for the EnT/ET-coexisting systems consisting of quantum dots and dye molecules.

*Author to whom correspondence should be addressed. E-mail: qunzh@ustc.edu.cn

DOI:10.1063/1674-0068/cjcp1905105

II. EXPERIMENTS

A. Materials

Reagent grades of *o*-phenylenediamine (*o*-PD), *m*-phenylenediamine (*m*-PD), rhodamine B (RhB), and polyvinylpyrrolidone (PVP, M_W=24000) were purchased from Sigma-Aldrich without further purification. Reagent grades of $NaBH_4$, ethanol, hexane, acetone, methylene chloride, methanol, and $H_2PtCl_6{\cdot}6H_2O$ were provided by Sinopharm Chemical Reagent Co., Ltd. without further purification.

B. Synthesis of samples

The *o*-CQDs and *m*-CQDs were prepared following a hydrothermal method reported elsewhere [15]. Briefly, 900 mg of *o*-PD (*m*-PD) was dissolved in 90 mL ethanol to form the *o*-PD (*m*-PD) solution, which was then transferred into a poly(tetrafluoroethylene)-lined autoclave. After being heated (180 °C for 12 h) and naturally cooled down to room temperature, the *o*-PD (*m*-PD) suspension in the color of orange (gray) was obtained. The two crude products were then purified with the silica column chromatography using a mixture of methylene chloride and methanol as the eluent. After removing the solvents and further drying under vacuum, we obtained two purified products of *o*-CQDs and *m*-CQDs. Subsequently, we obtained the composite system of *o*-CQDs (*m*-CQDs)/RhB by stirring the mixture of *o*-CQDs (*m*-CQDs) (144 mg/L) and RhB (16 μmol/L) in ethanol for 3 h, similarly to the procedure in a previous report [16].

Another composite system of CQDs/Pt nanoparticles (NPs) was also prepared to aid the identification of the ET-related observations in the CQDs/RhB systems. The Pt NPs were synthesized via the following procedures. Briefly, 50 mg of PVP and 100 mL of 1 mmol/L $H_2PtCl_6{\cdot}6H_2O$ (in deionized water) were mixed in a conical flask under vigorous stirring and then 1 mL of 170 μmol/L $NaBH_4$ solution was added. The homogeneous solution was stirred for 30 min and then the as-synthesized PVP-protected Pt NPs were precipitated by acetone and centrifuged at 8000 r/min for 5 min. After being washed with acetone/hexane to remove excess PVP, the Pt NPs were re-dispersed in deionized water to form a colloidal solution for further use. Subsequently, the composite system of *o*-CQDs/Pt NPs was acquired by stirring the mixture of *o*-CQDs (144 mg/L) and Pt NPs (23 mg/L) in ethanol for 10 min.

C. Characterizations

The transmission electron microscopy (TEM) images were acquired on a JEM-2100F system. The X-ray photoelectron spectroscopy (XPS) measurements were performed on a Thermo Scientific ESCALAB 250 X-ray photoelectron spectrometer. The Mott-Schottky measurements were conducted on an electrochemical station (CHI-660D). The steady-state ultraviolet-visible (UV-Vis) absorption spectra were recorded on a TU-1901 spectrophotometer (Persee). The steady-state photoluminescence (PL) emission spectra were recorded on an FLS920 fluorescence spectrometer (Edinburgh). The PL quantum yields were measured using a C13534 UV-NIR absolute PL quantum yield spectrometer (Hamamatsu).

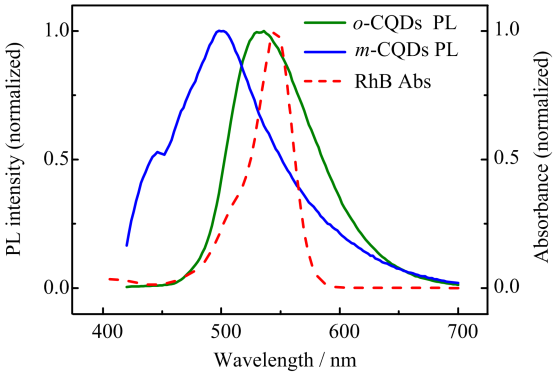

FIG. 1 The normalized steady-state PL spectra of *o*-CQDs and *m*-CQDs (solid lines) as well as the normalized steady-state UV-Vis absorption spectrum of RhB (dashed line).

The ultrafast transient absorption (TA) measurements were performed on a Helios pump-probe system (Ultrafast Systems LLC) under ambient conditions. The 400-nm pump pulses (∼60 nJ/pulse at the sample cell) were provided by the frequency doubling of the 800-nm output from a Ti:sapphire regenerative amplifier (Coherent). The white-light continuum probe pulses (450−600 nm) were generated by focusing the 800-nm beam (split from the regenerative amplifier, ∼400 nJ/pulse) onto a sapphire plate. The instrument response function was determined to be ∼100 fs by a routine cross-correlation procedure. The temporal and spectral profiles (chirp-corrected) of the pump-induced absorbance change (ΔA) of the samples were registered using an optical fiber-coupled multichannel spectrometer and further processed by a Surface Xplorer software. The samples well dispersed in ethanol were contained in a 0.7-mL quartz cuvette under a continuous magnetic stirring condition ensuring that the photoexcited volume of the samples was kept fresh during the TA measurements.

III. RESULTS AND DISCUSSION

All of the synthesized *o*-CQDs, *m*-CQDs, and Pt NPs turned out to be well dispersed in ethanol with a spherical shape and a few-nanometer size, as shown in their TEM images (FIG. S1 in supplementary ma-

DOI:10.1063/1674-0068/cjcp1905105

terials). The XPS spectra (FIG. S2 in supplementary materials) revealed the elemental compositions of the two CQDs mainly contain carbon, nitrogen, and oxygen. Their excellent organic solubility originates from the existence of O- and N-containing groups on the surface. As for the steady-state UV-Vis spectra (FIG. S3 in supplementary materials), the two broad profiles of *o*-CQDs peaking at around 260 and 430 nm can be linked to the $\pi\rightarrow\pi^*$ and $n\rightarrow\pi^*$ transitions, respectively [17]; while the two major peaks of *m*-CQDs at around 300 and 350 nm can be ascribed to the $n\rightarrow\pi^*$ transitions of C=O and C=N, respectively [18, 19].

FIG. 1 shows the normalized steady-state PL spectra (under 400-nm excitation) of *o*-CQDs (peaking at 536 nm) and *m*-CQDs (peaking at 498 nm) together with the normalized steady-state absorption spectrum of RhB (peaking at 546 nm). A substantial amount of spectral overlap exists between *o*-CQDs PL emission and RhB absorption, while that between *m*-CQDs PL emission and RhB absorption is smaller. Given that the EnT efficiency usually depends on the extent of spectral overlap between donor emission and acceptor absorption [20, 21], the above observation suggests that the efficiency of EnT in *o*-CQDs/RhB (*o*-CQDs as the donor and RhB as the acceptor) would be higher than that in *m*-CQDs/RhB (*m*-CQDs as the donor and RhB as the acceptor). FIG. 2(a) shows the PL spectra of bare *o*-CQDs, bare RhB, and *o*-CQDs/RhB under 400-nm excitation. It is worth noting that the concentrations of *o*-CQDs and RhB in *o*-CQDs/RhB were deliberately kept identical with those of bare CQDs (144 mg/L) and bare RhB (16 μmol/L) in the PL measurements. In order to calibrate against the influence of excitation light intensity, the PL spectra of bare *o*-CQDs and bare RhB shown in FIG. 2(a) were recorded with different intensities, *i.e.*, 87% and 13% of a certain intensity I_0, respectively, where I_0 was the intensity at which the PL spectrum of *o*-CQDs/RhB shown in FIG. 2(a) was recorded. The intensity percentages of 87% and 13% were determined from the observed absorbances (at 400 nm) of *o*-CQDs and RhB in *o*-CQDs/RhB, respectively, as listed in Table S1 (supplementary materials). Obviously, the straightforward superposition of the PL profiles of bare *o*-CQDs and bare RhB cannot produce that of *o*-CQDs/RhB, implying the existence of interactions between them. In terms of the two predominant PL peaks of *o*-CQDs/RhB, the one mainly contributed by *o*-CQDs (peaking at around 520 nm) is suppressed while the other mainly contributed by RhB (peaking at around 580 nm) gets significantly enhanced, clearly indicating the occurrence of a high-efficiency EnT process from the donor *o*-CQDs to the acceptor RhB. Similarly to the system of *o*-CQDs/RhB, the EnT process can also be identified in the system of *m*-CQDs/RhB (see the relevant PL spectra in FIG. 2(b)).

We now evaluate the EnT efficiencies in the two systems of *o*-CQDs/RhB and *m*-CQDs/RhB, without consideration of the ET process for the moment. According

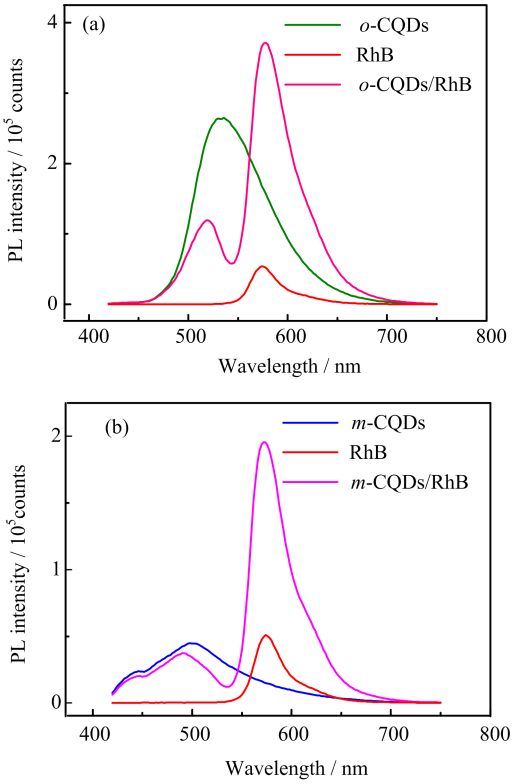

FIG. 2 The steady-state PL spectra of (a) *o*-CQDs, RhB, and *o*-CQDs/RhB and (b) *m*-CQDs, RhB, and *m*-CQDs/RhB.

to the Förster formalism [22], the EnT efficiency (η) can be estimated by

$$\eta = 1 - \frac{F}{F_0} \tag{1}$$

where F_0 (F) is the PL intensity of the donor in the absence (presence) of the acceptor, and can also be expressed in the form of

$$\eta = \frac{{R_0}^6}{({R_0}^6 + r^6)} \tag{2}$$

where r is the donor-acceptor distance and R_0 is the critical distance at which the EnT efficiency reaches 50%. R_0 can be calculated by

$$R_0 = \left(8.8 \times 10^{-25} K^2 n^{-4} \phi_{\mathrm{D}} J(\lambda)\right)^{1/6} \tag{3}$$

where the spatial orientation factor K^2 and the refraction index n (ethanol) are 2/3 and 1.36, respectively, according to a recent report [23]. The quantum yields ϕ_{D} of *o*-CQDs and *m*-CQDs were determined to be 10.2% and 3.1%, respectively, from the PL absolute quantum yield measurements. The spectral overlap integral $J(\lambda)$

DOI:10.1063/1674-0068/cjcp1905105

can be calculated by

$$J(\lambda) = \frac{\int F_{\mathrm{D}}(\lambda)\varepsilon_{\mathrm{A}}(\lambda)\lambda^4 \mathrm{d}\lambda}{\int F_{\mathrm{D}}(\lambda)\mathrm{d}\lambda} \quad (4)$$

where F_{D} is the donor's PL intensity and ε_{A} is the acceptor's molar extinction coefficient. In the system of *o*-CQDs/RhB, the $J(\lambda)$ value was estimated to be 3.80×10^{-13} $\mathrm{cm^3\cdot L\cdot mol^{-1}}$ based on the PL spectrum of *o*-CQDs in the spectral range of 450−600 nm (see FIG. 1) and Eq.(4). The R_0 value can thus be calculated to be 4.33 nm according to Eq.(3). On the other hand, the η value can be experimentally determined to be 73.2% according to Eq.(1), in which the F_0 value was directly from the integral of the PL profile of bare *o*-CQDs (FIG. 2(a)) and the F value was derived from the portion of PL profile of *o*-CQDs in *o*-CQDs/RhB (see the shaded region in FIG. S4(a) in supplementary materials). As such, the r value can be calculated to be 3.66 nm according to Eq.(2). Similarly, the η, $J(\lambda)$, R_0, and r values can also be determined for the *m*-CQDs/RhB system on the basis of the spectroscopic observations (see FIG. 1, FIG. 2(b), and FIG. S4(b) in supplementary materials) and the above equations. Table I summarizes the key parameters acquired for the two EnT systems in the context of Förster model. It turned out that the EnT efficiency in the *o*-CQDs/RhB system (73.2%) is more than twice that in the *m*-CQDs/RhB system (33.5%).

The above EnT efficiencies were acquired without taking account of the ET process between CQDs and RhB. To assess the possibility that the ET process may also occur in the two CQDs/RhB systems, we need to examine the relevant energetics of the two CQDs relative to RhB. FIG. 3 exhibits the relative energies (*vs.* NHE, pH=0) of the highest occupied molecular orbital (HOMO) and the lowest unoccupied molecular orbital (LUMO) for the three species, in which the HOMO/LUMO energy levels of the two CQDs were determined from the Mott-Schottky measurements and Tauc plots (details in FIG. S5 and its accompanying note in supplementary materials) while those of RhB were taken from Ref.[24]. Thermodynamically, the ET process from the donor CQDs to the acceptor RhB can occur in the two systems in principle, as illustrated by the arrows in FIG. 3.

Thus we further resorted to femtosecond time-resolved TA spectroscopy [6, 25, 26] to track in real time the photoexcited electron dynamics, in an attempt to visualize the ET-related behavior in the two systems. A pump-probe scheme with a UV pump (400 nm) and a white-light continuum probe (450−600 nm) were adopted. The representative TA spectra recorded on the two bare CQDs and on the two composite systems of CQDs/RhB at several probe delays are displayed in FIG. S6 (supplementary materials), in which the broad,

TABLE I The key parameters acquired for the two EnT systems in the context of Förster model.

System	$J(\lambda)/(\mathrm{cm^3\cdot L\cdot mol^{-1}})$	R_0/nm	r/nm	η
o-CQDs/RhB	3.80×10^{-13}	4.33	3.66	73.2%
m-CQDs/RhB	2.52×10^{-13}	3.32	3.72	33.5%

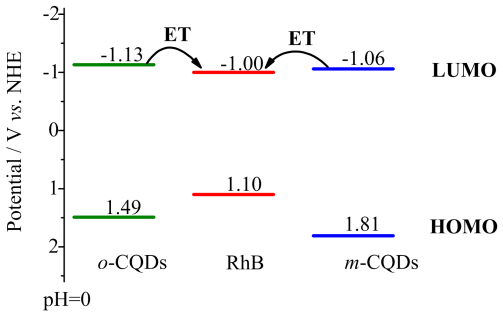

FIG. 3 The energy-level diagram for the three bare samples of *o*-CQDs, RhB, and *m*-CQDs.

positively-valued and negatively-valued TA profiles correspond to photoinduced absorption (PA) and photoinduced bleaching (PB), respectively. The PB signals observed in the two CQDs/RhB systems are mainly contributed by RhB, as readily proven by the comparison between FIG. S6 and FIG. S7 (*i.e.*, the TA spectra recorded on bare RhB under otherwise the same conditions as in FIG. S6). It is worth noting that there exists an isobestic point at 491 nm in the TA spectra of bare RhB (FIG. S7 in supplementary materials), which offers an ideal probing slot for looking into the PA evolution without interference of the TA signals from bare RhB; in other words, monitoring the PA kinetics at 491 nm would be neatly linked to the CQDs in the composite systems of CQDs/RhB. Here a question arises: what is the PA evolution displayed in FIG. S6 responsible for? To answer this question, we deliberately constructed another composite system of *o*-CQDs/Pt NPs in which RhB was replaced with Pt NPs. As is well known, Pt NPs can serve as a highly efficient electron acceptor to induce accelerated kinetics of photoexcited electrons in many semiconductor/Pt NPs composite systems, due to the opening of an additional ET pathway through which the photoexcited electrons can be effectively channeled to and accumulated on Pt NPs [6, 27]. As expected, we observed such an effect in the *o*-CQDs/Pt NPs system (details in FIG. S8 and its accompanying note in supplementary materials). On the basis of the above control and comparison experiments, we can safely conclude that the PA evolution displayed in FIG. S6 originates from the photoexcited electrons of CQDs.

We now turn our attention to comparing the TA kinetics (probed at 491 nm) of bare *o*-CQDs *vs.* *o*-CQDs/RhB (FIG. 4(a)) and bare *m*-CQDs *vs.* *m*-CQDs/RhB (FIG. 4(b)). Table II collects the relaxation time constants derived from the tri-exponential fit of the ob-

DOI:10.1063/1674-0068/cjcp1905105

TABLE II The relaxation time constants derived from the tri-exponential fit of the observed kinetics (pump: 400 nm, probe: 491 nm) for the four investigated systems.

System	τ_1/ps	τ_2/ps	τ_3/ps	τ_{ave}/ps
o-CQDs	3.6±0.4 (15.8%)	165±11 (22.3%)	>4000 (61.9%)	
o-CQDs/RhB	3.4±0.7 (18.3%)	168±22 (19.5%)	>4000 (62.2%)	
m-CQDs	2.9± 0.1 (58.0%)	31±3 (24.2%)	249±20 (17.8%)	211±17
m-CQDs/RhB	2.5±0.1 (55.1%)	16±2 (22.5%)	140±8 (22.4%)	123±7

Note: The corresponding statistical weights from the tri-exponential fitting are given in the parentheses.

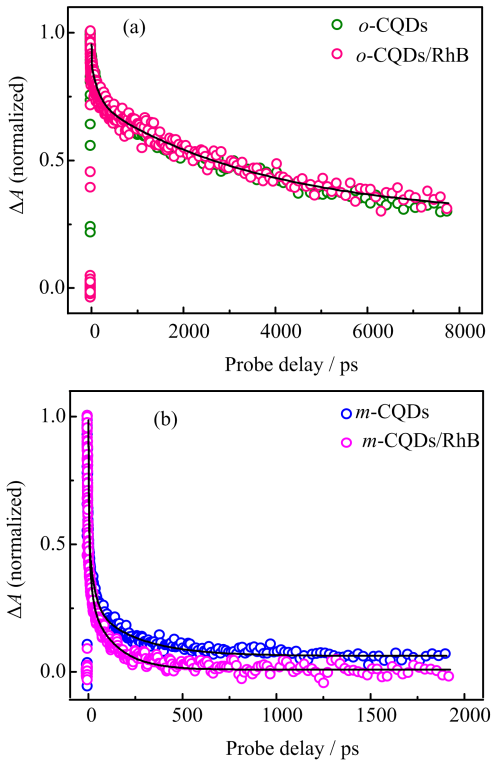

FIG. 4 The comparison of the TA kinetics (pump at 400 nm and probe at 491 nm) of (a) *o*-CQDs *vs.* *o*-CQDs/RhB and (b) *m*-CQDs *vs.* *m*-CQDs/RhB.

served kinetics for the four investigated systems. The τ_1 and τ_2 processes can be ascribed to the two consecutive pathways of exciton relaxation to two trap states with different trap depths while the τ_3 process is ascribed to the eventual electron-hole recombination [28]. Note that all of the relaxation time of bare *m*-CQDs is shorter than that of bare *o*-CQDs, reflecting their intrinsic difference in the distribution of O- and N-containing functional groups on the surface. As for the comparison of *o*-CQDs and *o*-CQDs/RhB, no discernible variation in their kinetics can be observed, indicating that the ET process from *o*-CQDs to RhB is negligible. As for the comparison of *m*-CQDs and *m*-CQDs/RhB, however, one can detect pronounced acceleration in the τ_2 and τ_3 processes for the latter relative to the former. On average, the relaxation lifetime of *m*-CQDs and *m*-CQDs/RhB is about 211 and 123 ps, respectively. Such a roughly 1.7-fold reduction in average lifetime can certainly be correlated with the opening of an additional ET channel from *m*-CQDs to the nearby RhB molecules, revealing that the ET process in the *m*-CQDs/RhB system cannot be neglected at all, unlike the situation in the *o*-CQDs/RhB system.

As demonstrated by the PL characterizations and analyses (FIG. 2 and FIG. S4 in supplementary materials), the exciton quenching effect exists in both systems of *o*-CQDs/RhB and *m*-CQDs/RhB but with different efficiencies. As for the *o*-CQDs/RhB system, since the ET process is negligible, the η value of 73.2% derived from the Förster model properly characterizes the EnT efficiency. As for the *m*-CQDs/RhB system, however, the η value of 33.5% obviously overvalues the EnT efficiency because of the occurrence of pronounced ET process. As the EnT and ET rates exhibit r^{-6} and exponential dependences, respectively, the latter is much more sensitive to the donor-acceptor distance r than the former [22, 29]. At long distances the EnT rate is usually much larger than the ET rate. The estimated donor-acceptor distance of about 3.7 nm for both systems (based on our PL characterizations) could be a certain long distance through which ET is less competitive than EnT in the exciton quenching processes. At such a long distance between the CQDs donor and the RhB acceptor, the ET process gets suppressed given a sufficiently high EnT efficiency (∼73.2%), as observed in the *o*-CQDs/RhB system, while it becomes significant when the EnT efficiency (<33.5%) is not that high, as observed in the *m*-CQDs/RhB system.

IV. CONCLUSION

In summary, the energy transfer (EnT) and electron transfer (ET) processes as well as their relationship in the *o*-CQDs/RhB and *m*-CQDs/RhB systems have been investigated by means of steady-state absorption, photoluminescence, and ultrafast transient absorption spectroscopy. In the *o*-CQDs/RhB system with a sufficiently high EnT efficiency (∼73.2%), the ET process turns out to be suppressed; while in the *m*-CQDs/RhB system with a much lower EnT efficiency (<33.5%), the ET process becomes significant. The understanding on

DOI:10.1063/1674-0068/cjcp1905105

such an interplay between the EnT and ET processes would offer useful inputs for applications based on the EnT/ET-coexisting systems comprising quantum dots and dye molecules.

Supplementary materials: TEM images, XPS spectra, steady-state UV-Vis absorption spectra, steady-state PL spectra, Mott-Schottky plots, Tauc plots, and ultrafast TA spectra of the samples are available.

V. ACKNOWLEDGMENTS

This work was supported by the National Key Research and Development Program on Nano Science and Technology of MOST (No.2016YFA0200602 and No.2018YFA0208702), the National Natural Science Foundation of China (No.21573211 and No.21633007), and the Anhui Initiative in Quantum Information Technologies (AHY090200).

[1] C. H. M. Chuang, P. R. Brown, V. Bulović, and M. G. Bawendi, Nat. Mater. **13**, 796 (2014).
[2] X. W. Gong, Z. Y. Yang, G. Walters, R. Comin, Z. J. Ning, E. Beauregard, V. Adinolfi, O. Voznyy, and E. H. Sargent, Nat. Photon. **10**, 253 (2016).
[3] M. Y. Ye, Z. H. Zhao, Z. F. Hu, L. Q. Liu, H. M. Ji, Z. R. Shen, and T. Y. Ma, Angew. Chem. Int. Ed. **56**, 8407 (2017).
[4] E. Oh, M. Y. Hong, D. Lee, S. H. Nam, H. C. Yoon, and H. S. Kim, J. Am. Chem. Soc. **127**, 3270 (2005).
[5] A. P. Litvin, E. V. Ushakova, P. S. Parfenov, A. V. Fedorov, and A. V. Baranov, J. Phys. Chem. C 118, 6531 (2014).
[6] X. G. Li, W. T. Bi, L. Zhang, S. Tao, W. S. Chu, Q. Zhang, Y. Luo, C. Z. Wu, and Y. Xie, Adv. Mater. **28**, 2427 (2016).
[7] L. Chen, L. Zhang, S. L. Jiang, and Q. Zhang, Chin. J. Chem. Phys. **31**, 165 (2018).
[8] R. Roy, S. Hohng, and T. Ha, Nat. Methods **5**, 507 (2008).
[9] A. M. Funston, J. J. Jasieniak, and P. Mulvaney, Adv. Mater. **20**, 4274 (2008).
[10] S. Sadhu, K. K. Haldar, and A. Patra, J. Phys. Chem. C **114**, 3891 (2010).
[11] S. Saha, D. Majhi, K. Bhattacharyya, N. Preeyanka, A. Datta, and M. Sarkar, Phys. Chem. Chem. Phys. **20**, 9523 (2018).
[12] A. Issac, S. Y. Jin, and T. Q. Lian, J. Am. Chem. Soc. **130**, 11280 (2008).
[13] S. Jagadeeswari, M. A. Jhonsi, A. Kathiravan, and R. Renganathan, J. Lumin. **131**, 597 (2011).
[14] Y. Yang, W. Rodríguez-Córdoba, and T. Q. Lian, Nano Lett. **12**, 4235 (2012).
[15] K. Jiang, S. Sun, L. Zhang, Y. Lu, A. G. Wu, C. Z. Cai, and H. W. Lin, Angew. Chem. Int. Ed. **54**, 5360 (2015).
[16] S. L. Hu, Q. Zhao, Q. Chang, J. L. Yang, and J. Liu, RSC Adv. **4**, 41069 (2014).
[17] P. D. Zhou, H. Liu, S. C. Chen, L. Lucia, H. Y. Zhan, and S. Y. Fu, Molbank **3**, M730 (2011).
[18] Y. X. Fang, S. J. Guo, D. Li, C. Z. Zhu, W. Ren, S. J. Dong, and E. K. Wang, ACS Nano **6**, 400 (2012).
[19] P. Wu, W. Li, Q. Wu, Y. S. Liu, and S. X. Liu, RSC Adv. **7**, 44144 (2017).
[20] S. A. Crooker, J. A. Hollingsworth, S. Tretiak, and V. I. Klimov, Phys. Rev. Lett. **89**, 186802 (2002).
[21] K. E. Sapsford, L. Berti, and I. L. Medintz, Angew. Chem. Int. Ed. **45**, 4562 (2006).
[22] J. R. Lakowicz, *Principles of Fluorescence Spectroscopy*, 2nd Edn., New York: Kluwer Academics (1999).
[23] V. R. Desai, S. M. Hunagund, M. S. Pujar, M. Basanagouda, J. S. Kadadevarmath, and A. H. Sidarai, J. Mol. Liq. **233**, 166 (2017).
[24] Q. Li, X. Li, S. Wageh, A. A. Al-Ghamdi, and J. G. Yu, Adv. Energy Mater. **5**, 1500010 (2015).
[25] Q. Zhang and Y. Luo, High Power Laser Sci. Eng. **4**, e22 (2016).
[26] Q. C. Shang, X. Z. Fang, H. L. Jiang, and Q. Zhang, Chin. J. Chem. Phys. **31**, 613 (2018).
[27] K. F. Wu, H. M. Zhu, Z. Liu, W. Rodríguez-Córdoba, and T. Q. Lian, J. Am. Chem. Soc. **134**, 10337 (2012).
[28] D. A. Wheeler and J. Z. Zhang, Adv. Mater. **25**, 2878 (2013).
[29] A. Boulesbaa, Z. Q. Huang, D. Wu, and T. Q. Lian, J. Phys. Chem. C **114**, 962 (2010).

DOI:10.1063/1674-0068/cjcp1905105